Electrochimica Acta 235 (2017) 527–533

Contents lists available at ScienceDirect

Electrochimica Acta

journal homepage: www.elsevier.com/locate/electacta

Self-doped TiO_2 nanotube electrodes: A powerful tool as a sensor platform for electroanalytical applications

Guilherme Garcia Bessegato[1,*], Felipe Fantinato Hudari[1], Maria Valnice Boldrin Zanoni

Universidade Estadual Paulista (Unesp), Instituto de Química, Araraquara, Av. Prof. Francisco Degni, 55, 14800-060, Araraquara, SP, Brazil

ARTICLE INFO

Article history:
Received 24 November 2016
Received in revised form 17 March 2017
Accepted 18 March 2017
Available online 20 March 2017

Keywords:
titanium dioxide
cathodic polarization
sensing platform
p-phenylenediamine oxidation
determination

ABSTRACT

The use of TiO_2 nanotube (TiO_2NTs) electrodes as anodes without UV irradiation has been described herein for electroanalytical purposes. Although semiconductors of *n*-type, such as TiO_2NTs, do not offer any potential electrochemical response at the anodic region, they can be "activated" once they are *a priori* subjected to a simple cathodic polarization (P-TiO_2NTs) and used to follow the oxidation reaction without any other modification. The best polarization conditions were obtained at 0.1 mol L^{-1} KH_2PO_4 pH 10 at −2.5 V for 5 min, and the polarized TiO_2 electrode was applied in the $Fe(CN)_6^{4-}$ redox probe oxidation and also *p*-phenylenediamine (PPD) determination as models of species which undergo oxidation. Following the optimization of the parameters, analytical curves for $Fe(CN)_6^{4-}$ and PPD were constructed in the range of 2.5×10^{-5} to 5×10^{-3} mol L^{-1} with a detection limit at 7.23×10^{-6} mol L^{-1} and 0.500 to 98.6×10^{-6} mol L^{-1} with a detection limit at 0.558×10^{-7} mol L^{-1} using linear sweep voltammetry and linear sweep adsorptive stripping voltammetry techniques, respectively. Lastly, the figures of merit for P-TiO_2NT and conventional glassy carbon electrodes are compared. Our results show that P-TiO_2NT electrodes can be used as an excellent platform for the development of electrochemical sensors.

© 2017 Published by Elsevier Ltd.

1. Introduction

Highly ordered nanomaterials such as TiO_2 nanotubes (TiO_2NT), can be easily prepared using electrochemical anodization, giving the titanium distinct advantages that allow its application in photoelectrocatalysis [1,2] such as dye-sensitised solar cells [3], water splitting [4] and oxidation of contaminants [5]. Nevertheless, their use as electroanalytical sensors without UV irradiation has been poorly explored to date, due largely to their semiconductive properties that hinder response at positive potentials [6]. The studies using TiO_2NT as anodic sensors require surface modifications with conductive elements including metallic nanoparticles and carbon compounds, such as Ag and graphene oxide [6], Pt [7,8], Ni [9], Pd, Pt and Au [10] and reduced graphene oxide [6]. Wang and collaborators developed a non-enzymatic amperometric glucose sensor based on a Pt nanoparticle-decorated TiO_2 nanotube array electrode. Through measurements in 0.1 mol L^{-1} NaOH solution by chronoamperometry, the linear range and detection limit found were $1–15 \times 10^{-3}$ mol L^{-1} and 0.2×10^{-3} mol L^{-1}, respectively [8]. In another study, Mahshid and co-authors developed a sensor based on the electrodeposition of Pd, Pt and Au nanoparticles in the TiO_2 nanotube electrodes for dopamine determination. Using differential pulse voltammetry technique, the linear range and detection limit were 5.0×10^{-8} to 3.0×10^{-5} mol L^{-1} and 3×10^{-8} mol L^{-1}, respectively [10].

A new class of TiO_2NT with improved electrochemical properties has been recently developed by simple cathodic polarization (electrochemically self-doped TiO_2NT). These works showed that self-doped TiO_2NT can be applied as supercapacitors [11–15], anodes for lithium ion batteries [16], anodes for the generation of oxidants [12,14,17,18], photoanodes in photoelectrochemical water splitting [19] and the degradation of contaminants [20,21]. These possibilities can be engendered by activating the TiO_2 semiconductor via self-doping once Ti^{3+} dopant states are created, leading to an almost metallic behavior of the material [15,22]. Nevertheless, there is no evidence that this kind of self-doping can generate a versatile surface of TiO_2 nanotubes which are useful in electroanalysis.

The present work seeks to demonstrate that it is remarkably feasible to use electrochemically self-doped TiO_2NTs as a sensing platform for monitoring electrochemical oxidation. The use of

* Corresponding author. Tel.: +55 1633019740.
E-mail addresses: guilhermebessegato@iq.unesp.br, guilhermebessegato@gmail.com (G.G. Bessegato), felipehudari@iq.unesp.br (F.F. Hudari), boldrinv@iq.unesp.br (M.V.B. Zanoni).

[1] These authors contributed equally.

http://dx.doi.org/10.1016/j.electacta.2017.03.141
0013-4686/© 2017 Published by Elsevier Ltd.

nanostructured morphology, such as nanotubes, commonly offers greater surface area and excellent electron percolation pathways for vectorial charge transfer between interfaces [1,11] enhancing the electroanalytical signal. Thus, at the heart of this work we sought to evaluate the TiO_2NT anodic response in relation to $Fe(CN)_6^{4-}$ and *p*-phenylenediamine (PPD) used as model compounds, showing new opportunities for the application of TiO_2 nanotube electrodes as sensing platforms.

2. Experimental

2.1. Preparation and characterization of TiO_2 self-doped nanotube electrodes

The TiO_2 nanotube electrodes (TiO_2NT) were prepared by electrochemical anodization, in an organic electrolyte which was composed of 0.25% ammonium fluoride (98%, Synth) in glycerol (99.5%, Synth) containing 10% water, in compliance with the methodologies that have already been published in the literature [5]. A previously prepared Ti foil 0.5 mm thick and 2 × 1 cm was subjected to 30 V for 50 h. Then, the TiO_2NT electrode was washed and annealed at 450 °C for 60 min.

The self-doped TiO_2NT (P-TiO_2NT) electrodes were prepared by cathodic polarization in 0.1 mol L^{-1} KH_2PO_4 buffer. The effect of electrolyte pH (3, 7 and 10), applied potential (−1.5 V, −2.0 V and −2.5 V *vs* Ag/AgCl 3 mol L−1) and electrolysis time (5, 10 and 20 min) was evaluated. This step was carried out using an Autolab pgstat302N potentiostat, an Ag/AgCl (KCl 3 mol L^{-1}) as a reference electrode and a dimensionally stable anode (DSA, De Nora®) as a counter electrode. DSA® (mixed metal oxide) coatings are generally based on $IrO_2/RuO_2/TiO_2$ mixtures deposited on a metallic substrate (usually titanium) and are used because of their high overpotential for the oxygen evolution reaction. The performance of these electrodes was assessed vis-à-vis the electrochemical behavior of 5.0×10^{-3} mol L^{-1} $[Fe(CN)_6]^{4-}$ in 0.1 mol L^{-1} KCl solution, in order to choose the best polarization conditions. The geometric area of all electrodes was delimited to 0.276 cm^2.

The morphology and electrochemical response for both TiO_2NT and P-TiO_2NT were analyzed by X-ray diffraction (DRX), Field Emission Gun-Scanning Electron Microscopy (FEG-SEM), and electrochemical impedance spectroscopy (EIS). EIS analyses were conducted in an Autolab pgstat302N potentiostat with NOVA 1.11.2 software. EIS measurements were performed in 5.0×10^{-3} mol L^{-1} $Fe(CN)_6^{3-/4-}$ redox probe (0.1 mol L^{-1} KCl), between 10 kHz–0.03 Hz, with a 5 mV rms sinusoidal modulation at OCP, using an Ag|AgCl reference electrode and a Pt counter electrode. Mott-Schottky measurements were performed at a frequency of 10 Hz in 0.1 mol L^{-1} KH_2PO_4 buffer at pH 7. The electrolyte was bubbled with N_2 prior to these experiments.

2.2. Electroanalytical determination of $[Fe(CN)_6]^{4-}$ and PPD

As an inorganic model, the $[Fe(CN)_6]^{4-}$ electrochemical behavior on P-TiO_2NT was studied by cyclic and linear sweep voltammetry in 0.1 mol L^{-1} KCl electrolyte, at a scan rate of 100 mV s^{-1}. Cyclic and linear sweep voltammograms for *p*-phenylenediamine (model of organic compound) were carried out on P-TiO_2NT in 0.1 mol L^{-1} Britton-Robinson (B-R) buffer solution using a scan rate of 75 mV s^{-1}. The effect of pH (from 2 to 7), accumulation potential (−0.2, 0, 0.2 and 0.4 V) and accumulation time (0, 5, 10, 15 and 20 s) were all investigated in order to perform the experiments under the optimum conditions.

3. Results and Discussion

3.1. Characteristics of TiO_2NT and P-TiO_2NT electrodes

FEG-SEM images showed the formation of self-aligned nanotubes perpendicular to the metallic substrate with an average diameter of 80 nm, tube wall of 12 nm and length of 2.4 μm (Fig. 1a–c), after being grown by electrochemical anodization and annealing. In addition, polarized electrodes did not, in effect, show any morphological and crystallographic differences when compared to the original electrodes (Fig. 1b). The X-ray diffractograms (Fig. 1d) obtained for TiO_2NT presented no significant difference, while the peaks were indexed to the anatase phase formed after annealing at 450 °C [23].

Fig. 2a shows successive cyclic voltammograms (CVs) of a TiO_2NT electrode (without going through the process of cathodic polarization of the electrode) in 0.1 mol L^{-1} KH_2PO_4 electrolyte. In the first cycle (i), no anodic peak is observed from zero to 3.0 V, which was in line with our expectations when it comes to an *n*-type semiconductor without UV irradiation [24]. By so doing, the cathodic polarization at potentials negatively superior to −1.0 V leads to the accumulation of electrons on the semiconductor film, thereby causing the reduction of Ti^{4+} into Ti^{3+}. The electrochemical reduction is accompanied by charge compensation through the intercalation of protons $[Ti^{IV}O_2 + e^- + H^+ \leftrightarrows Ti^{III}(O)(OH)]$ [25,26]. The formation of high levels of Ti^{3+} dopant states (up to approx. 1% of the Ti^{4+} can be reduced to Ti^{3+}) [11] enables an almost metallic behavior of the material [15]. In addition, the density of hydroxyl groups on the surface of TiO_2 is increased, giving the material higher hydrophilic properties [22]. In the second cycle (ii), we

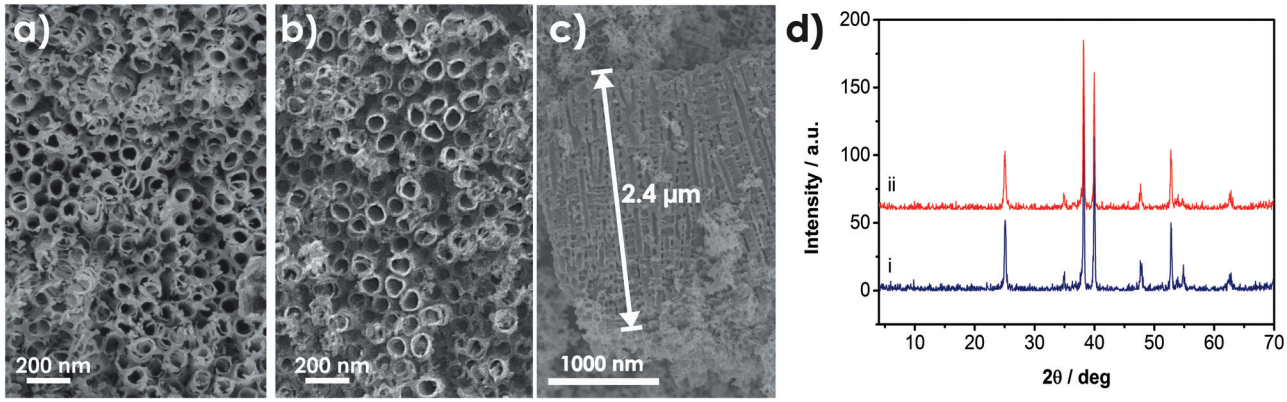

Fig. 1. FEG-SEM images for TiO_2NT a) before, b) after cathodic polarization; and c) side view of the TiO_2 nanotubes; d) X-ray diffractrogram of (i) TiO_2NT and (ii) P-TiO_2NT samples.

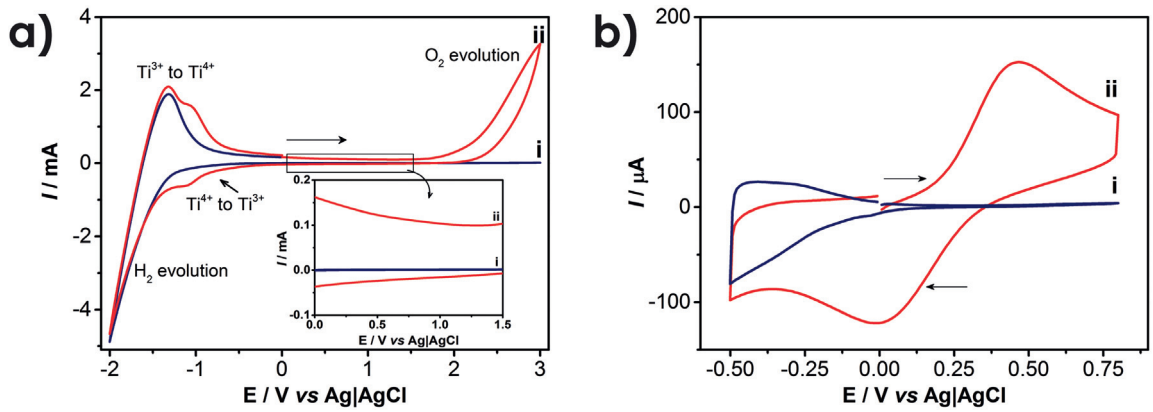

Fig. 2. (a) Successive cyclic voltammograms of a TiO_2NT in 0.1 mol L^{-1} KH_2PO_4 buffer (pH 10); (b) CV of TiO_2NT in 5.0×10^{-3}mol L^{-1} $[Fe(CN)_6]^{4-}$ in 0.1 mol L^{-1} KCl solution in 75 mV s^{-1}.

observed a relatively higher current, from zero to approximately +1.7 V, when the oxygen evolution was at its onset, demonstrating the "activation" of TiO_2 for anodic reactions, which was promoted after scanning the first cycle (i) at potentials lower than −1.0 V. This behavior is said to be irreversible [17] given that even after the oxidation of Ti^{3+} to Ti^{4+} at −1.3 V, P-TiO_2NT is found not to be deactivated while retaining a relatively higher conductivity compared to the first cycle. Successive cyclic voltammograms carried out between 0.0 and 2.0 V for P-TiO_2NT electrodes in 0.1 mol L^{-1} B-R buffer pH 2.0 (Supplementary material Fig. S1) showed unchanging voltammetric profile, which indicated stable performance.

Fig. 2b shows the respective cyclic voltammograms obtained for the oxidation of 5.0×10^{-3} mol L^{-1} $Fe(CN)_6^{4-}$ solutions in 0.1 mol L^{-1} KCl on TiO_2NT prior to (i) and following (ii) polarization for 5 min at −2.5 V and under pH 10. Before polarization (i), it is clear that there is no Fe^{2+} oxidation cycling from zero to 0.80 V, and the absence of the Fe^{3+} reduction peak during the cathodic sweep is also obvious. However, for the polarized electrode (ii), its new properties allowed the oxidation of Fe^{2+} to Fe^{3+} at 0.46 V and a reduction peak of Fe^{3+} to Fe^{2+} at 0.0 V. The difference between $E_{ap} - E_{cp} = 0.46$ V is 3 to 4 times higher than that observed for GCE [27,28]. In addition, the value of $I_{ap}/I_{cp} = 0.85$, suggests a slight deviation of a reversible process [29]. Nevertheless, their properties indicate that the P-TiO_2NT electrode can be employed as an electroanalytical sensor, showing unheard oxidation properties and enhanced reduction abilities.

EIS measurements (Nyquist plots) for both TiO_2NT and P-TiO_2NT in 5.0×10^{-3} mol L^{-1} $Fe(CN)_6^{3-/4-}$ are shown in Fig. 3a. On the other hand, Fig. 3b shows the equivalent circuit used to fit the EIS data, in agreement with Xiao et. al [30], in which R_1 represents the solution resistance (R_s) and the parallel combination of R_2CPE_2 is associated to the conductivity and capacitance of TiO_2 nanotubes. The parallel combination of R_3CPE_3 represents the interfacial ionic charge transfer resistance (R_{ct}) and the double layer capacitance (C_{dl}), such as in a Randles circuit. Table 1 shows the parameters determined by the fitting of the experimental EIS data using the Nova 1.11.2 software (Metrohm Autolab B.V.). The electrical resistance of the oxide film (R_2) increased from 0.880 kΩ in the P-TiO_2NT electrode to 2500 kΩ in the TiO_2NT electrode. It is worth noting that the value of CPE_2, which is higher for P-TiO_2NT, indicates superior capacitive properties provided by the cathodic polarization, which in turn attests their applicability as supercapacitors. Comparing the interfacial ionic charge transfer resistance (R_3), it decreases substantially for P-TiO_2NT (1.37 kΩ) (Fig. 3a, curve ii) in relation to the TiO_2NT electrode (72.5 kΩ) (curve i), implying much lower electron transfer resistance to the

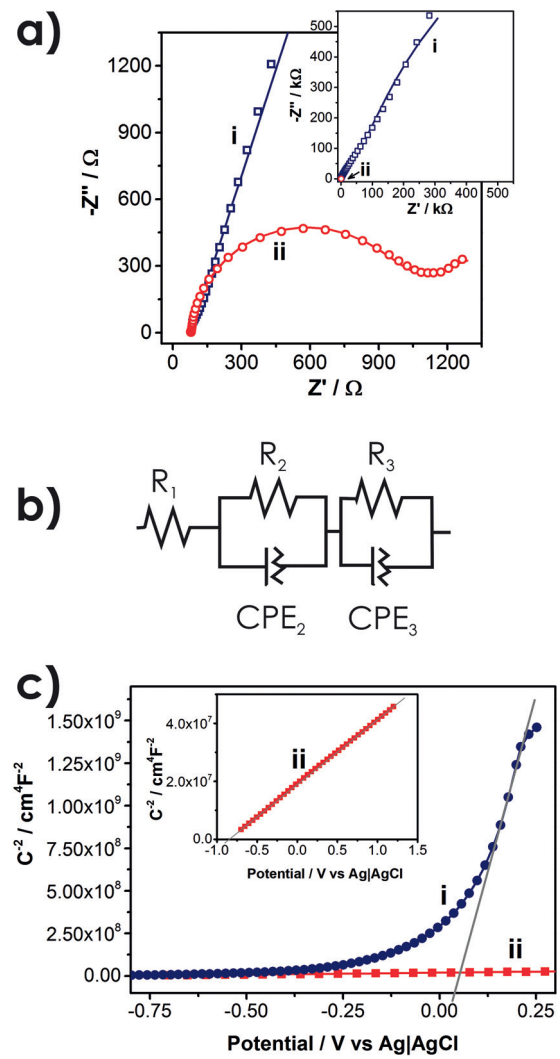

Fig. 3. (a) Nyquist plots in 5.0×10^{-3} mol L^{-1} $Fe(CN)_6^{3-/4-}$ redox probes for TiO_2NT; where (i) stands for prior to polarisation and (ii) indicates after cathodic polarization; (b) Proposed equivalent circuit for polarized samples and (c) C^{-2} *vs* *E* relation at 10 Hz in phosphate buffer pH 7.

redox probes in the electrolyte solution. This behavior was reported in previous studies when dealing with self-doped TiO_2NTs [11–13,17].

Potential-dependent capacity measurements (Mott-Schottky analyses) at 10 Hz in phosphate buffer pH 7 were used to estimate the carrier's densities, N_D, and the flatband potential, U_{fb}, for both samples (the phase angle vs. frequency plot, Bode plot, can be found in Fig. S2 of the Supplementary material). Assuming that the capacity of the of the space charge region of TiO_2 is much smaller than that of the Helmholtz layer, it follows the Mott-Schottky relationship [31]:

$$C_{SC}^{-2} = \left(\frac{2}{\varepsilon\varepsilon_0 e A^2 N_D}\right)\left(U - U_{fb} - \frac{kT}{e}\right) \quad (1)$$

Where C_{SC} represents the differential capacitance of the space charge layer, e is the elementary electron charge (1.6×10^{-19}C); ε_0 is the permittivity in vacuum (8.86×10^{-14} F cm^{-1}); ε is the dielectric constant (48 for anatase) [21]; U is the applied bias potential; U_{fb} is the flat band potential; k is the Boltzmann constant; T is the temperature; and A is the surface area (cm^2). The surface area was calculated assuming an idealized nanotubular structure, as previously demonstrated [32], resulting in 41.2 cm^2. Fig. 3c shows the Mott-Schottky plots obtained for both electrodes, demonstrating that the TiO_2NT electrode exhibits greater capacity dependence on the potential, due to the space charge layer and positive slopes, which are expected for an n-type semiconductor. However, the self-doped electrode (P-TiO_2NT) showed only a little dependence of capacitance on the applied potential, which is related to the Helmholtz layer at the semiconductor/electrolyte interface that exhibited semi-metallic behavior [33]. Thus, N_D can be calculated using the linear region slope of C^{-2} *vs.* U plot ($N_D = 2/\varepsilon \cdot \varepsilon_0 \cdot e \cdot A^2 \cdot slope$). Considering the line equations: $y = 7.28 \times 10^9 x - 2.35 \times 10^8$ ($R^2 = 0.9936$) and $y = 2.23 \times 10^7 x + 1.92 \times 10^7$ ($R^2 = 0.9998$), the calculated carrier densities (N_D) were 2.38×10^{17} and 7.78×10^{19} cm^{-3}, for TiO_2NT and P-TiO_2NT, respectively. This data is in agreement with previous results reported in literature [20,21], and show that polarized electrodes presented higher carrier density and improved charge transfer properties, attributed to the formation of oxygen vacancy states as a result of the self-doping process, which is also in agreement with the EIS data for the $Fe(CN)_6^{3-/4-}$ redox probe. In addition, the flat band potential can be determined from the intercept, U, on the potential axis ($U_{fb} = U - (kT/e)$). The U_{fb} for pristine TiO_2NT and P-TiO_2NT electrodes were evaluated to be +0.00 V and −0.88 V, respectively. The negative shift of the flat band potential for the self-doped TiO_2 occurs due to the formation of Ti^{3+} donor states (oxygen vacancies) in the TiO_2 band gap, which helps to move the Fermi level of P-TiO_2 towards the conduction band [34]. Furthermore, increase in N_D and the negative shift of Fermi level results in increased band bending at the TiO_2/electrolyte interface, which tends to enhance the surface charge transfer [21].

3.2. Optimization of conditions for cathodic polarization

The conditions of cathodic polarization for the best anodic signal in the $[Fe(CN)_6]^{4-}$ oxidation were investigated: electrolyte pH (3, 7 and 10), applied potential (−1.5 V, −2.0 V and −2.5 V *vs* Ag/AgCl 3 mol L^{-1}) and electrolysis time (5, 10 and 20 min). The respective voltammograms are shown in Fig. S3. The optimized conditions were achieved at pH 10, under −2.5 V for 5 min. The intercalation reaction is slower in alkaline electrolytes, which allows a more precise control of the reaction sequence [15]. At more negative potentials, stronger expansion of TiO_2 lattice occurs due to H^+ intercalation and H_2 evolution, which can in turn, lead to a greater extension of formation of oxygen vacancies in the P-TiO_2NTs. At sufficient potential, the polarization results in probable cleavage of Ti—O bonds to form oxygen vacancies, or may even lead to the destruction of the nanotubes [11].

Thus, our findings show that it is possible to attain a new and unexplored anodic response for TiO_2NT electrodes without requiring extra modifications by metal ion doping, polymers or graphene decoration, for instance [6–10]. The use of a simple cathodic polarization for 5 min at −2.5 V is essentially sufficient to get a sensor platform with anodic response and great potentiality in electroanalytical measurements. For the purpose of illustrating this behavior, the proposed method was applied towards the determination of $[Fe(CN)_6]^{4-}$ (as an inorganic model) and p-phenylenediamine (as an organic model), a precursor of hair dyeing formulations and aramid plastics and fibres, which are easily oxidized on glassy carbon electrodes [35,36].

3.3. Demonstration of the oxidative ability of P-TiO_2NT electrodes using the model compounds

3.3.1. Electrochemical oxidation of $Fe(CN)_6^{4-}$ at polarized P-TiO_2NT electrodes

The applicability of the proposed sensor was first evaluated for oxidation of the $Fe(CN)_6^{4-}$ complex ion. As shown in Fig. 2b, after a simple pre-activation of the electrode at cathodic potential is

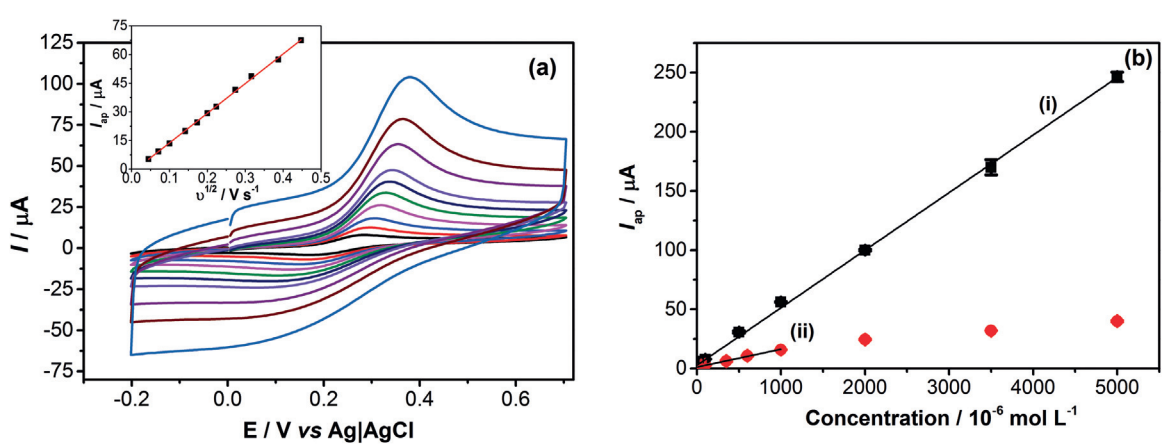

Fig. 4. (a) Cyclic voltammograms for 1.0×10^{-3} mol L^{-1} of $Fe(CN)_6^{4-}$ in the range 2 to 200 mV s^{-1} (Figure insert: relation between I_{ap} *vs.* $\nu^{1/2}$). (b) Linear relationship between I_{ap} *vs.* $Fe(CN)_6^{4-}$ concentration for (i) P-TiO_2NT electrodes in the range of 2.50×10^{-5}–5.00×10^{-3} mol L^{-1} and for (ii) GCE in the range of 5.00×10^{-5}–1.00×10^{-3} mol L^{-1} in 0.1 mol L^{-1} potassium chloride solution with scan rate of 75 mV s^{-1}.

Table 1
Impedance components for TiO_2NT and P-TiO_2NT electrodes fitted using the equivalent circuit shown in Fig. 3b. (EIS data obtained in 5.0×10^{-3} mol L^{-1} $Fe(CN)_6^{3-/4-}$ redox probe in 0.1 mol L^{-1} at OCP).

Electrode	R_1 (Ω)	R_2 (kΩ)	CPE_2-P	CPE_2-T (μF)	R_3 (kΩ)	CPE_3-P	CPE_3-T (μF)
TiO_2NT	79.2	2500	0.868	6.91	72.5	0.781	6.48
P-TiO_2NT	78.9	0.880	0.979	187	1.37	0.641	5190

possible to see a well-defined peak due oxidation of $Fe(CN)_6^{4-}$ to $Fe(CN)_6^{3-}$. The influence of scan rate in the anodic peak intensity (i_{ap}) was evaluated using cyclic voltammetry (Fig. 4a). The i_{ap} increased linearly from 2 to 200 mV s^{-1} following the equation $i_{ap} = 1.55 \times 10^{-4}\nu^{1/2} - 1.79 \times 10^{-6}$ ($R^2 = 0.998$) (Fig. 4a, inset), suggesting that the charge transfer is controlled by a diffusion process through the TiO_2 nanotubes pores [29]. For quantitative purposes, an analytical curve for $Fe(CN)_6^{4-}$ was constructed using the linear sweep voltammetry technique in 0.1 mol L^{-1} potassium chloride solution with a scan rate of 75 mV s^{-1} (Fig. 4b, curve (ii)). In these conditions, a linear relationship was found between 2.5×10^{-5} to 5×10^{-3} mol L^{-1} with the following equation $i_{ap} = 0.0486 \times [Fe(CN)_6^{4-}] + 2.61 \times 10^{-6}$ ($R^2 = 0.999$) (Fig. 4b, curve (i)).

The detection (LD) and quantitation (LQ) limits were calculated using the following equation: LD = 3 × *std*/m and LQ = 10 × *std*/m, where *std* is the standard deviation of 10 linear sweep voltammograms for supporting electrolyte (KCl solution 0.1 mol L^{-1}) and *m* is the slope of the equation of the calibration curve. The respective values for LD and LQ were 7.23 and 24.1×10^{-6} mol L^{-1}. The performance of the proposed sensor was compared to the voltammetric response for $Fe(CN)_6^{4-}$ oxidation at a glassy carbon electrode (GCE), a model of well-behaved electrode in anodic regions under the same experimental conditions (Fig. S4). An analytical curve for $Fe(CN)_6^{4-}$ using the GCE in the range between 5.00×10^{-5} and 1.00×10^{-3} mol L^{-1} is shown in Fig. 4b, curve ii, which represents a lower sensitivity than 3 times compared to the sensitivity when using the P-TiO_2NT electrode. Table 2 shows a comparison between the figures of merit for P-TiO_2NT and GCE.

For all parameters studied, the best values were observed for the proposed sensor, highlighting the sensitivity, which is a signal gain 3 times greater than when compared to GCE. Besides that, the repeatability of the method was verified after 10 consecutive analyses for the $Fe(CN)_6^{4-}$ solution at concentrations of 2.5×10^{-6} and 5.0×10^{-3} mol L^{-1}, where the relative standard deviation was 4.42 and 1.94%, respectively, indicating that the proposed electrode is not poisoned in consecutive tests since the solution is stirred between measurements.

3.3.2. Electrochemical oxidation of p*-phenylenediamine at polarized P-TiO_2NT electrode*

Fig. 5 illustrates the voltammetric profiles obtained for oxidation of 143×10^{-6} mol L^{-1} of *p*-phenylenediamine (PPD) on TiO_2NT prior to (i) and following polarization of the electrode (ii). As expected, no peak is observed for PPD oxidation on undoped TiO_2NT largely due to its *n*-type semiconductor properties. However, after polarization, a well defined anodic peak is observed at +0.632 V vis-à-vis the oxidation of the amine group of PDD [35].

The influence of scan rate (υ) in the range of 5 to 200 mV s^{-1} was investigated, where the anodic peak intensity (i_{ap}) of PPD was observed to increase following linear relationship for polarized electrodes ($i_{ap} = 6.90 \times 10^{-6}\ \upsilon^{1/2} - 2.54 \times 10^{-6}$ ($R^2 = 0.989$)), indicating that the mass transfer process is controlled by diffusion through the thin film of TiO_2 nanotubes [29]. This feature is found to be similar to the transport-like behavior observed in the redox process of solid state films [37,38] given the short range movements of redox sites within the film aiming at reaching a contact point.

It is noteworthy that these data indicate that P-TiO_2NT electrodes could be used as sensors in the monitoring of oxidizable compound. The electrochemical response was investigated and the best voltammetric signal was obtained using linear sweep adsorptive stripping voltammetry (LSAdSV) at pH 2 and under −0.2 V following 15 s of electrode preconditioning (data not shown).

Under optimized conditions, adsorptive stripping voltammetric curves were recorded and well defined peaks were found. It was observed that with increasing PPD concentration there is a shift in the anodic peak potential (E_{ap}) to more negative potentials. This behavior was previously observed by Xavier et al. [39] in the phenol oxidation. It was explained due to a more availability of phenoxy radical associated to a higher phenol concentration, which favors the oxidation reactions that occur at less anodic potentials. In the case of PPD, the even greater amount of *p*-phenylenediamine radical cations (or semiquinone radical) [40]

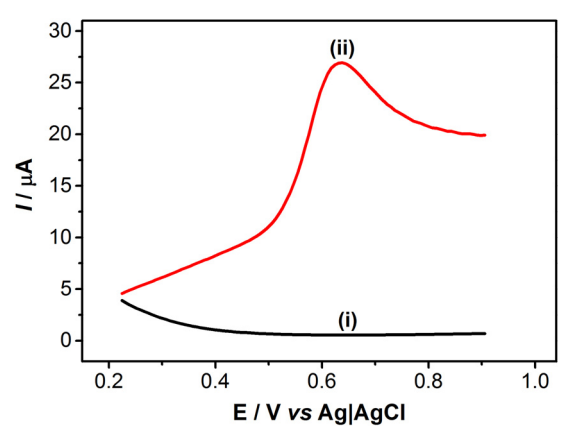

Fig. 5. Linear sweep voltammograms obtained for 143×10^{-6} mol L^{-1} of *p*-phenylenediamine in 0.1 mol L^{-1} B-R buffer solution using TiO_2NT electrodes (i) before and (ii) after cathodic polarisation. Scan rate of 75 mV s^{-1}.

Table 2
Comparison of figures of merit for $Fe(CN)_6^{4-}$ oxidation using P-TiO_2NT and GCE.

Parameters	P-TiO_2NT electrode	GCE
Linear relationship	2.50×10^{-5} to 5.00×10^{-3} mol L^{-1}	5.00×10^{-5} to 1.00×10^{-3} mol L^{-1}
Equation	$i_{ap} = 0.0486 \times [Fe(CN)_6^{4-}] + 2.61 \times 10^{-6}$	$i_{ap} = 0.0151 \times [Fe(CN)_6^{4-}] + 1.11 \times 10^{-6}$
R^2	0.999	0.986
LD	7.23×10^{-6} mol L^{-1}	11.3×10^{-6} mol L^{-1}
LQ	24.1×10^{-6} mol L^{-1}	37.6×10^{-6} mol L^{-1}

Table 3
Comparison of figures of merit for PPD using P-TiO_2NT and GCE.

Parameters	P-TiO_2NT	GCE
Linear relationship	0.500 to 98.6 × 10^{-6} mol L^{-1}	20 to 150 × 10^{-6} mol L^{-1}
Equation	i_{ap} = 0.402 × [PPD] + 3.71 × 10^{-8} (0.500 – 5.00 × 10^{-6} mol L^{-1}) i_{ap} = 0.190 × [PPD] + 1.50 × 10^{-6} (10.0 – 98.6 × 10^{-6} mol L^{-1})	i_{ap} = 0.0313 × [PPD] + 2.33 × 10^{-7}
R^2	0.990 (0.500 – 5.00 × 10^{-6} mol L^{-1}) 0.998 (10.0 – 98.6 × 10^{-6} mol L^{-1})	0.987
LD	0.0558 × 10^{-6} mol L^{-1}	5.92 × 10^{-6} mol L^{-1}
LQ	0.186 × 10^{-6} mol L^{-1}	19.7 × 10^{-6} mol L^{-1}

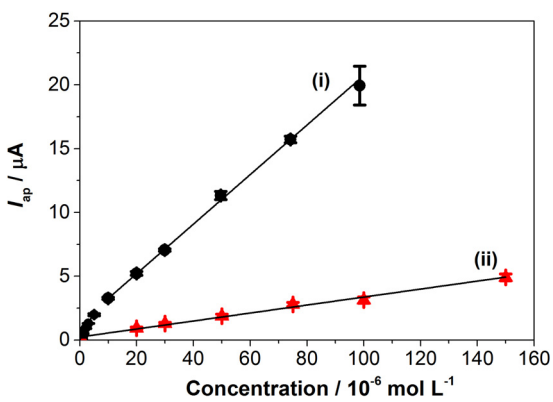

Fig. 6. Linear relationship between I_{ap} *vs.* concentration of *p*-phenylenediamine using (i) P-TiO_2NT electrode in the range of 0.500–5.00 × 10^{-6} mol L^{-1} and 10.0–98.6 × 10^{-6} mol L^{-1} and (ii) GCE in the range of 20–150 × 10^{-6} mol L^{-1} using LSAdSV.

resultant from the increasing PPD concentration in the analytical curve, is causing the potential shift.

In addition, the peak current i_{ap} increases with increasing PPD concentrations in the range of 0.500 to 98.6 × 10^{-6} mol L^{-1} presenting two linear regions in the range of 0.500–5.00 and 10.0–98.6 × 10^{-6} mol L^{-1} according to the following equations i_{ap} = 0.402 × [PPD] + 3.71 × 10^{-8} (R^2 = 0.990) and i_{ap} = 0.190 × [PPD] + 1.50 × 10^{-6} (R^2 = 0.998), respectively (Fig. 6, curve i). The limit of detection (LD) was 0.558 × 10^{-7} mol L^{-1} while the limit of quantification (LQ) was 1.86 × 10^{-7} mol L^{-1}. In order to test the potentiality of the proposed sensor platform for this model compound, an analytical curve was constructed and the figures of merit were calculated for PPD using GCE in the same above conditions (Fig. S5). Fig. 6 compares the calibration curves using the P-TiO_2NT (curve i) electrode and GCE (curve ii), which shows that our proposed sensor platform has highest sensitivity and lower values of LD and LQ.

Besides that, as shown in Table 3, for all the figures of merit, the best results were obtained using P-TiO_2NT electrode.

The repeatability of the measurements was tested recording linear scan voltammograms using 10 consecutive solutions containing concentrations of 1.00, 20.0 and 74.2 × 10^{-6} mol L^{-1} of PPD. The relative standard for P-TiO_2NT deviations were 4.25, 3.09 and 1.06%.

In addition to the comparison made above with the GCE, the LD and LQ values found for the polarized electrode are relatively lower compared to the LD and LQ obtained in other studies involving the determination of PPD [35,36], showing that the proposed sensor bear considerable advantages when it comes to the determination of substances at low levels, presenting better performance compared to some electrodes that require surface modification via methods which demand a relatively high time of modification besides the inherent difficulty that comes with them [36].

4. Conclusions

Our findings unfold another approach for TiO_2NT electrodes as electroanalytical sensors at anodic regions, with good performance in the case of $Fe(CN)_6^{4-}$ and PPD oxidation. The proposed method has been found to be easy, simple and is based on self-doping induced by cathodic polarization. This previous step is seen to be capable of promoting a dramatic increase in the conductivity and carriers density of TiO_2 nanotube electrodes. Furthermore, we find it essentially important and largely efficacious in that it allows the use TiO_2 nanotube arrays electrodes to monitor oxidative processes at anodic potentials without any UV irradiation. The TiO_2NT electrode can be used as an excellent platform for the development of electrochemical sensors with very good advantages, among them including low cost, easy fabrication, higher active surface area and fast electron transfer. While further studies are in progress to enable us fully understand the TiO_2 surface reactions, we believe the developed material has great potential for monitoring a broad range of substances; additional work is underway aimed at extending its application.

Acknowledgements

The authors are grateful to the Brazilian Research Agencies—FAPESP (grant numbers 2014/03679-7 and 2015/18109-4) and CNPq (grant numbers 153169/2014-1 and 446245/2014-3) for the financial support granted during the course of this research. FEG-SEM facilities were provided by LMA-IQ and X-Ray Diffraction measurements by GFQM-IQ.

Appendix A. Supplementary data

Supplementary data associated with this article can be found, in the online version, at http://dx.doi.org/10.1016/j.electacta.2017.03.141.

References

[1] C.A. Grimes, G.K. Mor, TiO_2 nanotube arrays: synthesis, properties, and applications, Springer, New York, 2009, doi:http://dx.doi.org/10.1007/978-1-4419-0068-5.
[2] P. Roy, S. Berger, P. Schmuki, TiO_2 nanotubes: synthesis and applications, Angew. Chemie Int. Ed. 50 (2011) 2904–2939, doi:http://dx.doi.org/10.1002/anie.201001374.
[3] M.A. Hossain, J. Park, J.Y. Ahn, C. Park, Y. Kim, S.H. Kim, et al., Investigation of TiO_2 nanotubes/nanoparticles stacking sequences to improve power conversion efficiency of dye-sensitized solar cells, Electrochim. Acta 173 (2015) 665–671, doi:http://dx.doi.org/10.1016/j.electacta.2015.05.141.
[4] N. Liu, S.P. Albu, K. Lee, S. So, P. Schmuki, Water annealing and other low temperature treatments of anodic TiO_2 nanotubes: a comparison of properties and efficiencies in dye sensitized solar cells and for water splitting, Electrochim. Acta 82 (2012) 98–102, doi:http://dx.doi.org/10.1016/j.electacta.2012.06.006.
[5] G.G. Bessegato, J.C. Cardoso, B.F. da Silva, M.V.B. Zanoni, Combination of photoelectrocatalysis and ozonation: a novel and powerful approach applied in Acid Yellow 1 mineralization, Appl. Catal. B: Environ. 180 (2016) 161–168, doi:http://dx.doi.org/10.1016/j.apcatb.2015.06.013.
[6] W. Wang, Y. Xie, C. Xia, H. Du, F. Tian, Titanium dioxide nanotube arrays modified with a nanocomposite of silver nanoparticles and reduced graphene

oxide for electrochemical sensing, Microchim. Acta 181 (2014) 1325–1331, doi:http://dx.doi.org/10.1007/s00604-014-1258-x.
[7] Y.-Y. Song, Z. Gao, K. Lee, P. Schmuki, A self-cleaning nonenzymatic glucose detection system based on titania nanotube arrays modified with platinum nanoparticles, Electrochem. Commun. 13 (2011) 1217–1220, doi:http://dx.doi.org/10.1016/j.elecom.2011.08.040.
[8] Y. Wang, J. Chen, C. Zhou, L. Zhou, Y. Kong, H. Long, et al., A novel self-cleaning, non-enzymatic glucose sensor working under a very low applied potential based on a Pt nanoparticle-decorated TiO_2 nanotube array electrode, Electrochim Acta 115 (2014) 269–276, doi:http://dx.doi.org/10.1016/j.electacta.2013.09.173.
[9] S. Yu, X. Peng, G. Cao, M. Zhou, L. Qiao, J. Yao, et al., Ni nanoparticles decorated titania nanotube arrays as efficient nonenzymatic glucose sensor, Electrochim. Acta 76 (2012) 512–517, doi:http://dx.doi.org/10.1016/j.electacta.2012.05.079.
[10] S. Mahshid, C. Li, S.S. Mahshid, M. Askari, A. Dolati, L. Yang, et al., Sensitive determination of dopamine in the presence of uric acid and ascorbic acid using TiO_2 nanotubes modified with Pd, Pt and Au nanoparticles, Analyst 136 (2011) 2322–2329, doi:http://dx.doi.org/10.1039/C1AN15021A.
[11] H. Zhou, Y. Zhang, Electrochemically self-doped TiO_2 nanotube arrays for supercapacitors, J. Phys. Chem. C 118 (2014) 5626–5636, doi:http://dx.doi.org/10.1021/jp4082883.
[12] C. Kim, S. Kim, J. Lee, J. Kim, J. Yoon, Capacitive and oxidant generating properties of black-colored TiO_2 nanotube array fabricated by electrochemical self-doping, ACS Appl. Mater. Interfaces 7 (2015) 7486–7491, doi:http://dx.doi.org/10.1021/acsami.5b00123.
[13] H. Zhou, Y. Zhang, Enhancing the capacitance of TiO_2 nanotube arrays by a facile cathodic reduction process, J. Power Sources 239 (2013) 128–131, doi:http://dx.doi.org/10.1016/j.jpowsour.2013.03.114.
[14] C. Kim, S. Kim, S.P. Hong, J. Lee, J. Yoon, Effect of doping level of colored TiO_2 nanotube arrays fabricated by electrochemical self-doping on electrochemical properties, Phys. Chem. Chem. Phys. 18 (2016) 14370–14375, doi:http://dx.doi.org/10.1039/C6CP01799A.
[15] J.M. Macak, B.G. Gong, M. Hueppe, P. Schmuki, Filling of TiO_2 nanotubes by self-doping and electrodeposition, Adv. Mater. 19 (2007) 3027–3031, doi:http://dx.doi.org/10.1002/adma.200602549.
[16] J. Duan, H. Hou, X. Liu, C. Yan, S. Liu, R. Meng, et al., In situ Ti^{3+}-doped TiO_2 nanotubes anode for lithium ion battery, J. Porous Mater. 23 (2016) 837–843, doi:http://dx.doi.org/10.1007/s10934-016-0139-6.
[17] C. Kim, S. Kim, J. Choi, J. Lee, J.S. Kang, Y.E. Sung, et al., Blue TiO_2 nanotube array as an oxidant generating novel anode material fabricated by simple cathodic polarization, Electrochim. Acta 141 (2014) 113–119, doi:http://dx.doi.org/10.1016/j.electacta.2014.07.062.
[18] Y. Yang, M.R. Hoffmann, Synthesis and stabilization of blue-black TiO_2 nanotube arrays for electrochemical oxidant generation and wastewater treatment, Environ. Sci. Technol. 50 (2016) 11888–11894, doi:http://dx.doi.org/10.1021/acs.est.6b03540.
[19] Z. Zhang, M.N. Hedhili, H. Zhu, P. Wang, Electrochemical reduction induced self-doping of Ti^{3+} for efficient water splitting performance on TiO_2 based photoelectrodes, Phys. Chem. Chem. Phys. 15 (2013) 15637, doi:http://dx.doi.org/10.1039/c3cp52759j.
[20] W. Liao, J. Yang, H. Zhou, M. Murugananthan, Y. Zhang, Electrochemically self-doped TiO_2 nanotube arrays for efficient visible light photoelectrocatalytic degradation of contaminants, Electrochim. Acta 136 (2014) 310–317, doi:http://dx.doi.org/10.1016/j.electacta.2014.05.091.
[21] Q. Zheng, H.-J. Lee, J. Lee, W. Choi, N.-B. Park, C. Lee, Electrochromic titania nanotube arrays for the enhanced photocatalytic degradation of phenol and pharmaceutical compounds, Chem. Eng. J. 249 (2014) 285–292, doi:http://dx.doi.org/10.1016/j.cej.2014.03.111.
[22] N. Sakai, A. Fujishima, T. Watanabe, K. Hashimoto, Highly hydrophilic surfaces of cathodically polarized amorphous TiO_2 electrodes, J. Electrochem. Soc. 148 (2001) E395–E398, doi:http://dx.doi.org/10.1149/1.1399279.
[23] G.G. Bessegato, J.C. Cardoso, M.V.B. Zanoni, Enhanced photoelectrocatalytic degradation of an acid dye with boron-doped TiO_2 nanotube anodes, Catal. Today 240 (2014) 100–106, doi:http://dx.doi.org/10.1016/j.cattod.2014.03.073.
[24] P.A. Carneiro, M.E. Osugi, J.J. Sene, M.A. Anderson, M.V.B. Zanoni, Evaluation of color removal and degradation of a reactive textile azo dye on nanoporous TiO_2 thin-film electrodes, Electrochim. Acta 49 (2004) 3807–3820, doi:http://dx.doi.org/10.1016/j.electacta.2003.12.057.
[25] Lyon L. Andrew, J.T. Hupp, Energetics of the nanocrystalline titanium dioxide/aqueous solution interface: approximate conduction band edge variations between $H_0 = -10$ and $H_- = +26$, J. Phys. Chem. B 103 (1999) 4623–4628, doi:http://dx.doi.org/10.1021/JP9908404.
[26] H. Pelouchova, P. Janda, J. Weber, L. Kavan, Charge transfer reductive doping of single crystal TiO_2 anatase, J. Electroanal. Chem. 566 (2004) 73–83, doi:http://dx.doi.org/10.1016/j.jelechem.2003.11.013.
[27] G. Orlandini, J. Groppi, A. Secchi, A. Arduini, J.D. Kilburn, Electrochemical response of the threading/de-threading process of calix[6] arene-based pseudorotaxanes anchored on glassy carbon electrodes, Electrochim. Acta 227 (2017) 391–400, doi:http://dx.doi.org/10.1016/j.electacta.2016.12.169.
[28] G. Zhao, Y. Yin, H. Wang, G. Liu, Z. Wang, Sensitive stripping voltammetric determination of Cd(II) and Pb(II) by a Bi/multi-walled carbon nanotube-emeraldine base polyaniline-Nafion composite modified glassy carbon electrode, Electrochim. Acta 220 (2016) 267–275, doi:http://dx.doi.org/10.1016/j.electacta.2016.10.059.
[29] A.J. Bard, L.R. Faulkner, Electrochemical methods: fundamentals and applications, 2nd ed., John Wiley & Sons, New York, 2001.
[30] P. Xiao, B.B. Garcia, Q. Guo, D. Liu, G. Cao, TiO_2 nanotube arrays fabricated by anodization in different electrolytes for biosensing, Electrochem. Commun. 9 (2007) 2441–2447, doi:http://dx.doi.org/10.1016/j.elecom.2007.07.020.
[31] A.G. Muñoz, Q. Chen, P. Schmuki, Interfacial properties of self-organized TiO_2 nanotubes studied by impedance spectroscopy, J. Solid State Electrochem. 11 (2007) 1077–1084, doi:http://dx.doi.org/10.1007/s10008-006-0241-9.
[32] S. Karthik, K.M. Gopal, E.P. Haripriya, Y. Sorachon, P. Maggie, K.V. Oomman, et al., Highly-ordered TiO_2 nanotube arrays up to 220 μm in length: use in water photoelectrolysis and dye-sensitized solar cells, Nanotechnology 18 (2007) 65707, doi:http://dx.doi.org/10.1088/0957-4484/18/6/065707.
[33] R. Hahn, F. Schmidt-Stein, J. Sahnen, S. Thiemann, Y. Song, J. Kunze, et al., Semimetallic TiO_2 nanotubes, Angew. Chemie Int. Ed. 48 (2009) 7236–7239, doi:http://dx.doi.org/10.1002/anie.200902207.
[34] J.W. Moir, E.V. Sackville, U. Hintermair, G.A. Ozin, Kinetics versus charge separation: improving the activity of stoichiometric and non-stoichiometric hematite photoanodes using a molecular iridium water oxidation catalyst, J. Phys. Chem. C 120 (2016) 12999–13012, doi:http://dx.doi.org/10.1021/acs.jpcc.6b00735.
[35] N.S. Lawrence, E.L. Beckett, J. Davis, R.G. Compton, Voltammetric investigation of hair dye constituents: application to the quantification of *p*-phenylenediamine, Analyst 126 (2001) 1897–1900, doi:http://dx.doi.org/10.1039/b104641c.
[36] F.F. Hudari, L.C. de Almeida, B.F. da Silva, M.V.B. Zanoni, Voltammetric sensor for simultaneous determination of *p*-phenylenediamine and resorcinol in permanent hair dyeing and tap water by composite carbon nanotubes/chitosan modified electrode, Microchem. J. 116 (2014) 261–268, doi:http://dx.doi.org/10.1016/j.microc.2014.05.007.
[37] N. Oyama, Factors affecting the electrochemical responses of metal complexes at pyrolytic graphite electrodes coated with films of poly(4-vinylpyridine), J. Electrochem. Soc. 127 (1980) 640, doi:http://dx.doi.org/10.1149/1.2129725.
[38] M. Noel, K.I. Vasu, Cyclic voltammetry and the frontiers of electrochemistry, Oxford & IBH Publishing, New Delhi, 1990.
[39] J.L.N. Xavier, E. Ortega, J.Z. Ferreira, A.M. Bernardes, V. Pérez-Herranz, An electrochemical study of phenol oxidation in acidic medium, Int. J. Electrochem. Sci. 6 (2011) 622–636.
[40] F. Cataldo, On the polymerization of *p*-phenylenediamine, Eur. Polym. J. 32 (1996) 43–50, doi:http://dx.doi.org/10.1016/0014-3057(95)00118-2.